Proceedings of ASME Turbo Expo 2019: Turbine Technical Conference and Exposition
GT2019
June 17-21, 2019, Phoenix, Arizona USA

GT2019-90452

NUMERICAL INVESTIGATION OF A SWIRL STABILIZED METHANE FIRED BURNER AND VALIDATION WITH EXPERIMENTAL DATA

Federica Farisco, Philipp Notsch

Institute of Thermal Turbomachinery and
Machine Dynamics
Graz University of Technology
8010 Graz, Austria
Email: federica.farisco@tugraz.at

Rene Prieler

Institute of Thermal Engineering
Graz University of Technology
8010 Graz, Austria

Felix Greiffenhagen, Jakob Woisetschlaeger, Franz Heitmeir

Institute of Thermal Turbomachinery and
Machine Dynamics
Graz University of Technology
8010 Graz, Austria

Christoph Hochenauer

Institute of Thermal Engineering
Graz University of Technology
8010 Graz, Austria

ABSTRACT

In modern gas turbines for power generation and future aircraft engines, the necessity to reduce NOx emissions led to the implementation of a premixed combustion technology under fuel-lean conditions. In the combustion chamber of these systems, extreme pressure amplitudes can occur due to the unsteady heat release, reducing component life time or causing unexpected shutdown events. In order to understand and predict these instabilities, an accurate knowledge of the combustion process is inevitable. This study, which was provided by numerical methods, such as Computational Fluid Dynamics (CFD) is based on a three-dimensional (3D) geometry representing a premixed swirl-stabilized methane-fired burner configuration with a known flow field in the vicinity of the burner and well defined operating conditions. Numerical simulations of the swirl-stabilized methane-fired burner have been carried out using the commercial code ANSYS Fluent. The main objective is to validate the performance of various combustion models with different complexity by comparing against experimental data. Experiments have been performed for the swirl-stabilized methane-fired burner applying different technologies. Velocity fluctuation measurements have been carried out and validated through several techniques, such as Laser Doppler Anemometry (LDA) and Particle Image Velocimetry (PIV). Laser Interferometric Vibrometry (LIV) provided information on heat release fluctuations and OH-chemiluminescence measurements have been done to identify the position of the main reaction zone. During the first part of the CFD investigation, the cold flow has been simulated applying different turbulence models and the velocity flow field obtained in the experiments has been compared with the numerical results. As next, the study focuses on the numerical analysis of the thermo-chemical processes in the main reaction zone. Few combustion models have been investigated beginning from Eddy Dissipation Model (EDM) and proceeding with increased complexity investigating the Steady Flamelet Model (SLF) and Flamelet Generated Manifold (FGM). An evaluation of the velocity field*

and temperature profile has been performed for all models used in order to test the validity of the numerical approach for the chosen geometry. The best option for future investigations of gas turbines has been identified.

NOMENCLATURE

D	Burner exit diameter	$[mm]$
d	Flame length above burner exit	$[mm]$
P_{th}	Thermal power	$[kW]$
T	Temperature	$[K]$
U	Velocity magnitude	$[m/s]$
U_t	Turbulent flame speed	$[m/s]$
u	Velocity component in x-coordinate	$[m/s]$
v	Tangential velocity component	$[m/s]$
Y_i	Mass fraction of species i	$[-]$
λ	Air/fuel ratio	$[-]$
ρ	Density	$[kg/m^3]$
Φ	Fuel/air ratio - equivalence ratio	$[-]$
CFD	Computational Fluid Dynamics	
CH_4	Methane gas	
CO_2	Carbon dioxide	
DES	Detached Eddy Simulation	
DO	Discrete Ordinates	
ED	Eddy Dissipation	
EDC	Eddy Dissipation Concept	
FGM	Flamelet Generated Manifold	
$ICCD$	Intensified Charge Coupled Device	
I_{OH*}	Light Intensity of OH*	
LES	Large Eddy Simulation	
LIV	Laser Interferometric Vibrometry	
LDA	Laser Doppler Interferometry	
PDF	Probability Density Function	
PIV	Particle Image Velocimetry	
$RANS$	Reynolds-Averaged Navier-Stoke	
RSM	Reynolds Stress Model	
SLF	Steady Laminar Flamelet	

INTRODUCTION

Lean premixed combustion technology is applied in modern gas turbine in order to reduce NO_x emissions providing a low flame temperature and high mixing quality. On the other hand it generates an important issue concerning combustion instabilities that need to be analyzed. Lean-premixed swirl-stabilized burners are the focus of the current study. In this work, a swirl-stabilized methane-air combustor configuration is investigated at atmospheric conditions with well known operating conditions. The flow field at the burner exit is obtained from Particle Image Velocimetry (PIV) data, and it is compared to CFD simulations in order to validate the numerical results. The main idea of the paper is to reproduce numerically the flow features of the swirl-stabilized methane-air combustor using RANS (Reynolds Averaged Navier Stokes) simulations as preliminary study for a following unsteady analysis. RANS methods are used in this work for a first representation and design of the combustion process.

The dynamics of the swirl-stabilized combustion process are described and explained in different papers (see [1] and [2]). Several methods for the measurement of the heat release are published [3, 4, 5] and the most common method used concerns the analysis of the chemiluminescence from OH* radicals within the flame. In the literature, studies (see [6, 7, 8]) can be found on different experimental techniques used to visualize the flame dynamics.

Prediction and analysis of combustor performances require detailed modeling and advanced measuring techniques [9]. In an industrial design process, RANS flow simulations, where the turbulent eddies are modeled and the time dependent fluctuations in the fluid flow are not considered, represent a standard tool that are able to capture the dominant flow features and benefit from the low computational time compared to LES or DES methods. Review papers by [9, 10, 11] provide an overview of recent progress based on numerical investigation of swirl-stabilized flames. In the previous work cited [10], various swirl stabilized burner geometries are investigated by several researchers testing different turbulence models. They came to the conclusion that the realizable k-ε model introduced by Shih et al. [12] performs best in such flows.

As second step the current paper arrives to discuss the numerical results obtained with various combustion models of different complexity. This study investigates the models ability to predict the behavior of the combustor analyzed in terms of temperature and species concentrations. In swirl-stabilized flames the interactions between chemistry and turbulence is complex. The coupling between turbulence and combustion is performed in the present paper through the CFD code Ansys Fluent v18.2 using combustion models, such as the combined EDM (Eddy Dissipation Model) introduced by Magnussen and Hjeertager [13], Steady Laminar Flamelet model (SLF) [14] and FGM. The work of [15] presents the results of numerical simulations with the realizable k-ε model and EDM showing an accurate reproduction of premixed combustion reactions of methane and air in nozzles. Magnussen [16] presents the Eddy Dissipation Concept Model (EDCM) as an extension of the EDM including detailed chemical mechanism of turbulent reacting flows in combustion systems. The work of Lysenko [17] compares SLF and EDCM for non premixed combustion applications. The study of [11] gives an accurate description of the Flamelet Generated Manifold (FGM) model and its application showing how this chemical reduction technique can represent an efficient modeling in premixed combustion. FGM, where a pre-computed laminar flamelet solution is integrated through a pre-defined probability density function (PDF) to account for turbulence effects, proved to be capable of

accurately describing the flame evolution since it can locally consider finite rate and non-equilibrium effects [18]. Anyway more accurate analysis is necessary to better understand and to gain knowledge in a deeper way concerning the limits of combustion modeling.
The aim of the current paper is to perform a numerical analysis of the combustion process reproduced by a laboratory test scale combustor in order to investigate the numerical models behavior through the evaluation of the velocity and temperature profiles. The application of the RANS approach is used as first design of the combustion process with the objective to perform as next step an unsteady analysis. The SLF applied in this paper has an added feature compare to the common SLF model used in Fluent. In the current SLF approach an additional equation for the reaction progress variable is added but without reaction progress variance. The originality of the paper lays on the application of a hybrid model with features between SLF and FGM that results in a more accurate representation of the experiments compared to the other models analyzed.

Combustor geometry analyzed

The configuration studied consists of a geometry burner with a thermal power of 3.44 kW. The burner reproduced in Fig 1 is described in detail in the work of Giuliani [19] and Peterleithner [5]. This configuration is referred to a premixed state [5]. Figure 2 shows the entire geometry of the methane burner investigated, including the burner exit region where the flame develops, taken as cylindrical shape for the computational domain. The burner presents six axial and tangential air inlets and four fuel supply lines around the circumference which are not used in the premixed operation mode. Both tangential and axial air are premixed with fuel in the outer mixing chamber and then they are transported into the plenum through a swirler, which consists of 32 cylindrical tubes aligned tangentially and symmetrically around the burner axis. Due to the radial and axial pressure gradients generated, a recirculation zone is formed which lowers the turbulent inflow velocity of the mixture. This stabilizing effect causes the flame to burn in a stable position and it ensures sufficient heat to ignite the fuel-oxidizer mixture [20]. The burner exit has a diameter of D=18 mm. In addition, 360 small cooling air openings (hole diameter of 5 mm and hole spacing of 5 mm) are distributed around the burner exit for dilution of the gases. The entire structure of the swirl-stabilized methane burner is documented in the work of Giuliani, Woisetschläger and Leitgeb [19].

Experimental setup

PIV

The experimental velocity profile is obtained by Particle Image Velocimetry (PIV) with the same setup as in [5]. The average

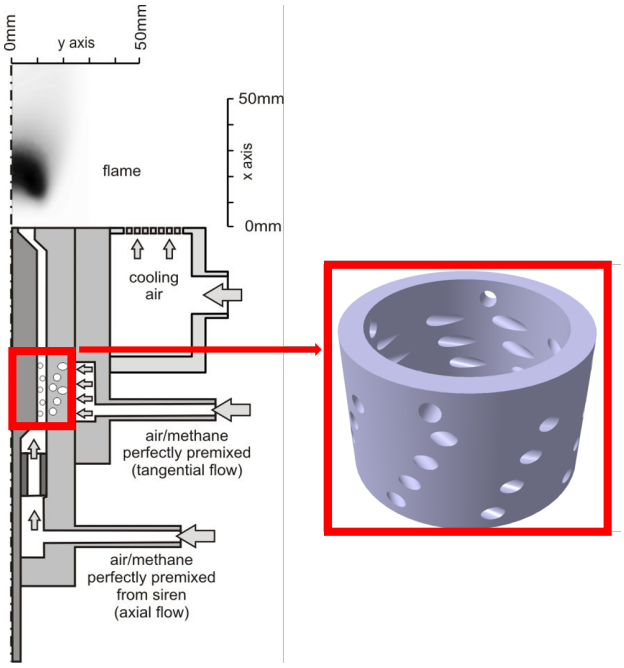

FIGURE 1. BURNER GEOMETRY: SCHEMATIC BURNER SECTION WITH DETAIL OF THE SWIRLER

is calculated out of 1200 images, the angle between the two cameras is 45°C.

Chemiluminescence

The OH* chemiluminescence images are recorded with an intensified charge coupled device (ICCD) camera and a 310 nm bandpass filter. Background subtraction as well as a corner shading correction are performed. The average emission is calculated from 6400 single images. Since the flame shows a radial symmetric behavior [21], local data are derived via Abel-transform [22] from the line-of-sight data recorded with the ICCD.

Background oriented Schlieren

Local gradients in density between an object and the observer lead to refraction of light, resulting in a distorted image. When calculating the cross-correlation between such an image and an undisturbed image with constant density, a density gradient proportional displacement can be obtained [23]. The integration of these gradients along the horizontal direction results in a density proportional field along the line-of-sight. Local data are calculated via tomographic reconstruction or Abel-transform if radial symmetry is assumed. Finally a calibration factor is needed to get absolute values from the arbitrary local density proportional values. This can be done by measuring temperature at different positions, which is then related to density via the ideal gas equation. The measurements shown in Fig. 8(a) are

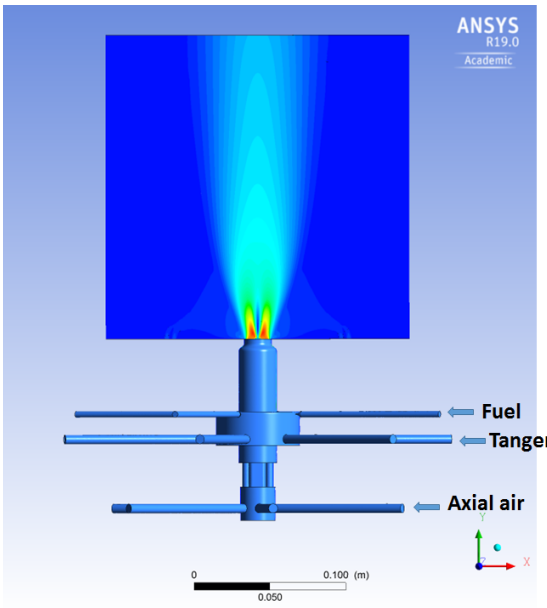

FIGURE 2. SKETCH OF THE BURNER AND COMPUTATIONAL DOMAIN

derived by averaging 1000 images. A random dot-pattern is used as background, in order to calculate a cross correlation between the undisturbed and the shifted dots.

Computational model

In this work different meshes are generated and a mesh independency study is performed. The commercial tool ANSYS mesher is applied for the generation of the meshes. A mesh study of the burner is done starting from a basic mesh with 13 million cells. The first cell-center of the coarsest mesh is located at an average non-dimensional wall distance of y^+=3. The coarsest mesh is refined successively arriving to two other versions with about 19 and 25 million cells in order to test the sensitivity of the solution. All generated meshes are used for the calculations with the cold flow and the realizable k-ε turbulence model. To rank the influence of the different mesh resolutions a global parameter, the swirl number, is analyzed. A simplified form of the swirl number equation is used. The simplified form is taken according to the experiments [8]. The same method for the calculation of the swirl number applied in the experiments is used also in the numerics to obtain a more accurate comparison between the two approaches. Two swirl numbers at fixed positions of the solid angle in the x-direction and in the z-direction are determined, respectively in positive and negative direction in a specific axial y-position integrated, which are shown in Equ. (1) and Equ. (2). The outer diameter of the burner outlet is chosen as integral boundaries based on recommendations in the literature [8].

$$S_x = \frac{2\int_{-r}^{r} wvx^2 dx}{D\int_{-r}^{r} v^2 x dx} \tag{1}$$

$$S_z = \frac{2\int_{-r}^{r} uvz^2 dz}{D\int_{-r}^{r} v^2 z dz} \tag{2}$$

By arithmetic averaging of the two values determined by means of Equ. (3), it is possible to determine the swirl number in a specific axial y-position of the methane burner. It is determined at three different positions: at the burner outlet, at a height of d=9 mm and at d=18 mm above the outlet. The swirl number values evaluated at the outlet of the burner and at d=9 mm show an accurate agreement with the swirl numbers gained from the experiments. The averaged swirl number calculated for all meshes presents a value S=0.44 that is slightly below the value of S=0.47 obtained in the experiments with a deviation of 6%.

$$S = \frac{S_x + S_z}{2} \tag{3}$$

	Swirl number	*Velocity v [m/s]*
Experiments	0.47	4
Mesh cells 13 (in Mio.)	0.44	4.5
Mesh cells 19 (in Mio.)	0.44	4.5
Mesh cells 24 (in Mio.)	0.44	4.5

TABLE 1. MESHES COMPARISONS

Details of mesh cells number, swirl number calculated and highest tangential velocity v values obtained are shown in Tab.1. The coarser mesh shows the same error in terms of swirl number compared to the finer meshes but it ensures less computational time steps than the other meshes. For this reason the mesh with the 13 million cells is chosen. A detail of the mesh used for the simulations with cold flow and different turbulence models is shown in Fig. 3. For the simulations with different combustion models a smaller mesh of 3 million cells consisting of few burner millimeters and the whole outlet burner cylinder is chosen due to computational time reason (see Fig. 4). The radial and axial velocity profiles are taken from the cold flow simulation at the interface (see Fig. 4) of the burner and applied as boundary conditions for the combustion simulations (black domain in Fig. 4) on the smaller domain of 3 million cells.

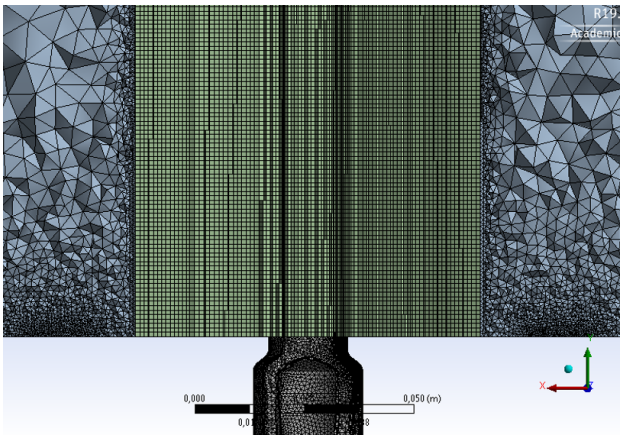

FIGURE 3. DETAIL OF THE SELECTED MESH

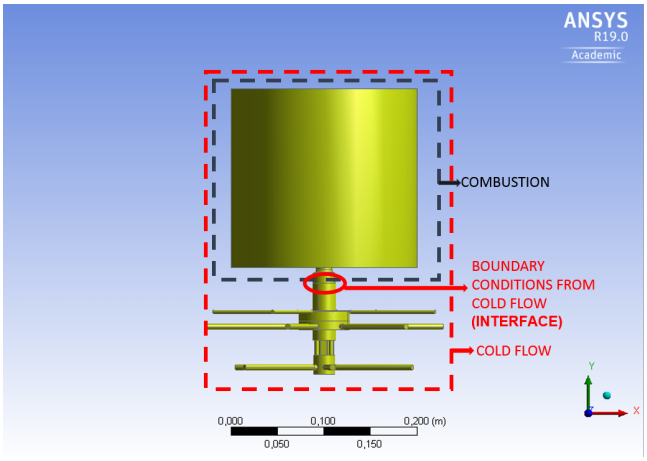

FIGURE 4. MESH AND BOUNDARY CONDITIONS USED IN COLD FLOW AND COMBUSTION SIMULATIONS

Figure 3 shows the cells shape used for the generation of the meshes. Structured hexahedral (hex)-cells are applied in the outlet burner region where the flame develops, and where high accuracy of the solution is needed due to the presence of high velocity, temperature, and species gradients. The hex mesh is preferred over tetrahedral-mesh since the hex-cells generate lower numerical dissipation (the mesh cells are in line with the general flow direction) and lower cell number (see [9]). A hexahedral mesh is not adopted also in the burner because it consists of a very complex geometry with very small pipes diameters (especially in the swirler) and it is easier to model with tetrahedral elements. The swirl number calculated and the velocity fields in Fig. 5 and Fig.6 show a good agreement compared to the experiments and it can be justified the usage of the tetra mesh in the burner. The outer cylinder of the burner, which includes the cooling air openings is modeled also with larger tetrahedral elements. Furthermore, prism layers are created at the edges of the methane burner, to solve the near-wall regions as accurately as possible.

Numerical Method

For all simulations presented in this paper steady state reacting RANS equations are applied based on the CFD code ANSYS Fluent, in order to predict the fluid flow and combustion process. The SIMPLE approach for pressure-velocity coupling is employed. For the spatial discretization, the second order upwind method is used instead of the quadratic upwind scheme $QUICK$ for momentum, turbulent kinetic energy and specific dissipation rate, since this leads to a more stable behavior of the simulation. The numerical simulations present a duration of the calculations up to about 40000 iterations steps. Residuals are observed during running time for mass, momentum, energy, CH_4 and CO_2. Few monitor points are located in different positions along the burner exit to check the convergence with respect to temperature, velocity and species concentrations.

Boundary conditions

The operating conditions of the burner test rig used in the experiments are taken for the numerical investigations. This allows comparisons between the measurement techniques applied and the numerical results. The study is performed for a fixed global equivalence ratio of $\Phi=\frac{1}{\lambda}=0.66$, with λ fixed air excess factor, at constant thermal power of P_{th}=3.44 kW. The value of the density in the cold flow simulation is assumed to be constant, since this remains almost unchanged and it represents an important aspect only in the combustion simulation. By specifying the mass flow and temperature at each inlet, as well as assuming atmospheric pressure at the exit of the combustor, the system is fully defined. The shortened mesh variant has only one inlet in the axial direction, composed of the premixed mass flows of fuel, axial and tangential air. The combustor walls are set as pressure outlet boundaries with ambient pressure in order to reproduce the experimental case where the flame is unconfined. The Discrete Ordinates (DO) model is used in all simulations to take into account the thermal radiation. For the tests performed enhanced wall treatment is applied to model the near-wall flow (see [24] and [25]) and the condition of y^+=3 is satisfied in refined regions of the combustion chamber walls.

Turbulence-chemistry interaction modeling

The chemistry of methane-air combustion involves many elementary reaction and species. In CFD simulations, the number of species needs to be limited in order to reduce the computational time. Different reaction mechanisms for methane-air mixture exist in literature (see the works [26], [27] and [28]). In this paper a two-step mechanism implemented in Fluent and introduced by Westbrook [29] is used for the ED simulation. For

the flamelet approaches the formulation described by the GRI-3.0 detailed mechanism of methane combustion with air is taken into account. It was introduced by Smith et al. [30] for the combustion of hydrocarbons and validated in the literature.

Different turbulence models are studied starting from the realizable k-ε with enhanced wall treatment, until Transition SST, arriving to Reynolds stress model (RSM) that should consider the effects of curvature, anisotropy and rotation in a more accurate way compared to the eddy viscosity turbulence models. The k-ε based models are frequently used for many practical turbulence flow analysis due to their robustness and simplicity compared to the more complex SST and RSM models. The standard k-ε model is a robust two-equation turbulence model that takes into account kinetic energy and dissipation rate. The realizable k-ε model is an improvement over the standard one, concerning flows with strong streamline curvature, vortices and rotation (see [15]).

Concerning the combustion modeling, in the current paper the Eddy Dissipation Model is tested and compared with the FGM and SLF flamelet methods. In the flamelet approaches the turbulent flame front is modeled by laminar flames where the flamelet equations are solved to obtain temperature, species concentration and density at each point in the main reaction zone of the laminar flamelet. The state between fuel and oxidant is given by the mixture fraction and the scalar dissipation. A following Probability Density Function (PDF) is used to couple the instantaneous values for the temperature and species from the flamelet calculation with the turbulent fluid flow. The PDF is defined as the fraction of time in which the fluid is in a certain state and it is identified by the mean mixture fraction and its variance [25]. For both approaches, FGM and SLF, diffusion flamelets are chosen as structure for the flamelets to generate the manifold. Turbulent Flame Speed-Zimont is taken for the progress variable source. In SLF a Turbulent Flame Speed Constant of $U_t = 0.52$ is mantained. In FGM the value of Turbulent Flame Speed Constant is changed to $U_t = 0.345$ in order to modify the flame position. As Turbulence-chemistry interaction a transport equation is used for the reaction progress variance in FGM. In ANSYS Fluent, the Zimont Turbulent Flame Speed closure is computed using a model for wrinkled and thickened flame fronts shown in Equ. 4, where A is a model constant, u' the RMS (root-mean-square) velocity, U_l laminar flame speed, α unburnt thermal diffusivity and l_t turbulence length scale.

$$U_t = A(u')^{\frac{3}{4}} U_l^{\frac{1}{2}} \alpha^{-\frac{1}{4}} l_t^{\frac{1}{4}} \tag{4}$$

As previously mentioned, in the SLF model applied in this paper an additional equation for the reaction progress variable C is added but without reaction progress variance $C' = 0$. The general SLF formulation without C equation included was also tested but the outcomes are not shown because not accurate and suited for a non-premixed model. All results presented in the current study are for partially premixed model. This hybrid approach with features between SLF and FGM results in a more accurate representation of the experiments compared to the other models analyzed.

Results discussion

Cold flow with different turbulence models

Figure 5 shows the absolute velocity field obtained numerically with cold flow and the three turbulence models compared with the experimental results. Half of the velocity field (radial section) is presented for clearer comparability with the experimental tests (x=0 burner axis). Figure 5(a) represents the experimental case with combustion. The area change at the burner exit causes a slight velocity deceleration due to swirl induced jet opening. The flow accelerates at around d=20 mm due to the expansion of the hot gases in the reaction zone and it decelerates gradually starting from d=35 mm for the mixing with the ambient gases. The measurements data can be used as a good approximation to validate the cold flow simulations in the range up to d=20 mm, highlighted by the black rectangle in Fig. 5(a). In the reaction zone range beyond d=20 mm the gas expansion generates increased absolute and tangential velocities that are not present in the cold flow simulations in Fig. 5(b), Fig. 5(c) and Fig. 5(d). Instead the range up to d=20 mm could be used to compare experiments with numerical results because the flow field is influenced by swirl induced jet opening present for the fluid flow with combustion and without (cold flow). Also the phenomenon of the precession of the cold vortex flow at specific frequency can be not considered in the current swirling flow case. This vortex cannot be reproduced in the experiments because results are obtained as average of time series data and in the numerics only RANS simulations are performed. Unsteady simulations will be carried out as following step of the current preliminary study.

The case with the realizable k-ε as turbulence model in Fig. 5(b), shows the highest magnitude velocity values in the range $U = \sqrt{u^2 + v^2}$=4-6 m/s up to about d=17 mm and it represents a good approximation with the experimental investigations. The velocity values in the cold flow decrease up to U=3 m/s beyond d=20 mm above the burner exit. The combustion process is not taken into account in the numerical cases with different turbulence models. For this reason any gas mixture expansion that could influence velocity and pressure fields is not present [8]. The numerical velocity profile is more aligned with the central axis compared to the experiments. The incoming flow is accelerated and broken or deflected at the front of the flame, as it can be observed in the experimental test. This deflection depends on the incoming swirl flow angle and the density differences between educts and products. A greater deflection of the flow can be observed with a larger density ratio between reactans and products

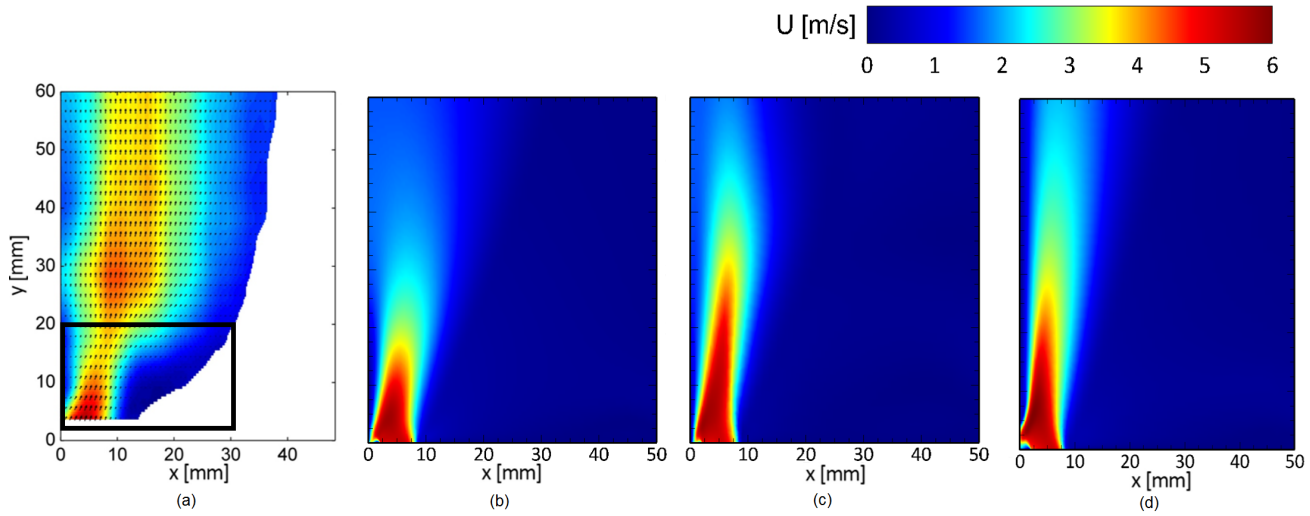

FIGURE 5. COLD FLOW COMPARISONS - ABSOLUTE VELOCITY PROFILE SHOWN FOR THE TURBULENCE MODELS (a) EXPERIMENTS, (b) $K-\varepsilon$, (c) SST AND (d) RSM

and with a constant flow angle [31].

The averaged swirl number calculated for this simulation with the realizable k-ε presents a value S=0.44 that is slightly below the value of S=0.47 obtained in the experiments with a deviation of 6%. The swirl number values evaluated at the outlet of the burner and at d=9 mm show an accurate agreement with the swirl numbers gained from the experiments. The discrepancy of the swirl number values measured at d=18 mm could be related to the different radius for the swirl number calculation and to the fact that the flame influence is not considered.

The simulation with the turbulence model Transition SST in Fig. 5(c) presents high absolute velocity values in the range of U=4-6 m/s up to d=30 mm, showing in the range d=10-20 mm much higher values than the measurements.

The averaged swirl number of the burner has approximately the same value as in the simulation with the k-ε model. The velocity field presented in the SST simulation can probably be attributed to the selected turbulence model, that could lead to turbulence overproduction in zones with large strain, as areas with acceleration. This could provoke the differences in the values obtained for this model compared to the realizable k-ε [25].

The absolute velocity profile for the RSM model in Fig. 5(d) also presents increased values in the range between d=10-20 mm in the axial direction compared to the simulation with the realizable k-ε model. This simulation shows a behavior that deviates from the experiments. This can probably be attributed to the model RSM that gives the best approximation for a strong swirl flow contrary to the current burner case that presents a moderate swirl. The turbulence model realizable k-ε model achieves the most accuarate agreement with the experiments [25] and it delivers considerable results in terms of velocity magnitude as well as the swirl number.

Simulations with different combustion models

Figures 6 and 7 present the absolute and tangential velocity profiles obtained from the simulations with the realizable k-ε and the three combustion models analyzed in this work. The numerical velocity contours are discussed and compared with the experimental results in Fig. 6(a) and Fig. 7(a).

Figure 6(b) shows the absolute velocity contour for the ED model, where the main reaction zone takes place at the central axis close to the burner exit. This phenomenon is related to the fast chemistry feature on which the ED model is based on. The absolute velocity profile represents an acceptable approximation to the experiments. A narrow shape of the velocity contour can be observed at the burner exit and it is due to the swirl-induced jet opening. The combustion process and the resulting gas expansion generate an opening of the velocity profile beyond d=20 mm. The velocity values up to about d=10 mm show a good agreement with the measurements. The numerical values are too high in the axial range d=10-20 mm. The main reaction zone is observed in the experiments at axial position d=25 mm, contrary to the numerical case that presents lower velocity values at a distance d=20-40 mm from the burner exit. This is related to the selected combustion model, where the combustion occurs when the reactants come into contact with each other and it takes place mainly in the area near the burner outlet. The tangential velocity profiles show a similar behaviour in the numerical cases that present an accurate agreement with the experiments in the range up to d=15 mm. SLF carries out higher velocity values compared to the other models beyond d=15 mm.

Figure 8 shows the numerical temperature profiles compared

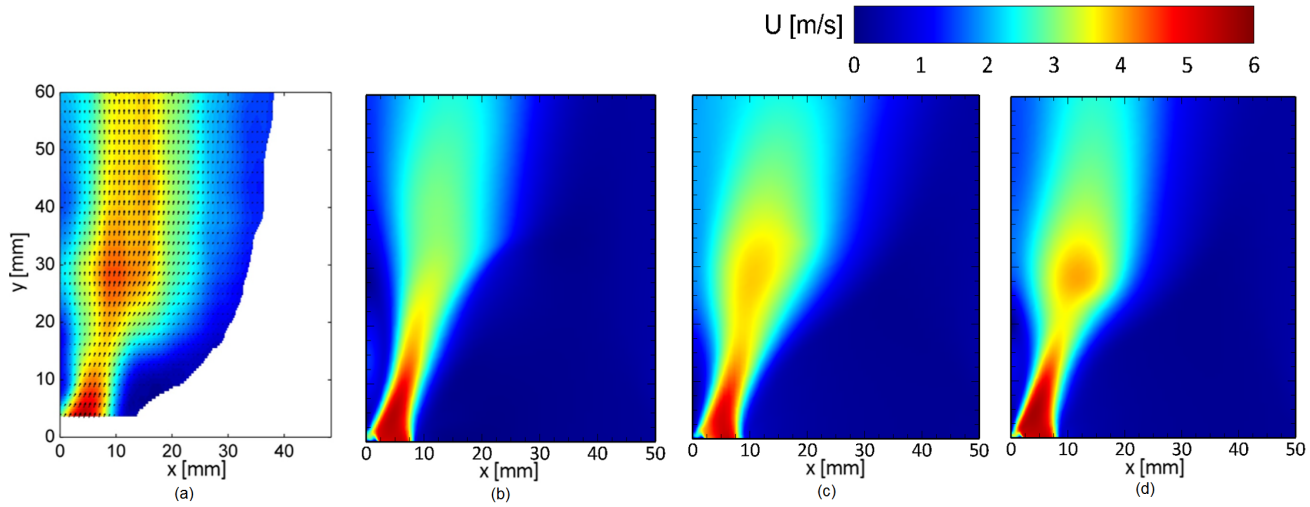

FIGURE 6. FLOW COMPARISONS - ABSOLUTE VELOCITY PROFILE SHOWN FOR THE COMBUSTION MODELS (a) EXPERIMENTS, (b) ED, (c) FGM AND (d) SLF

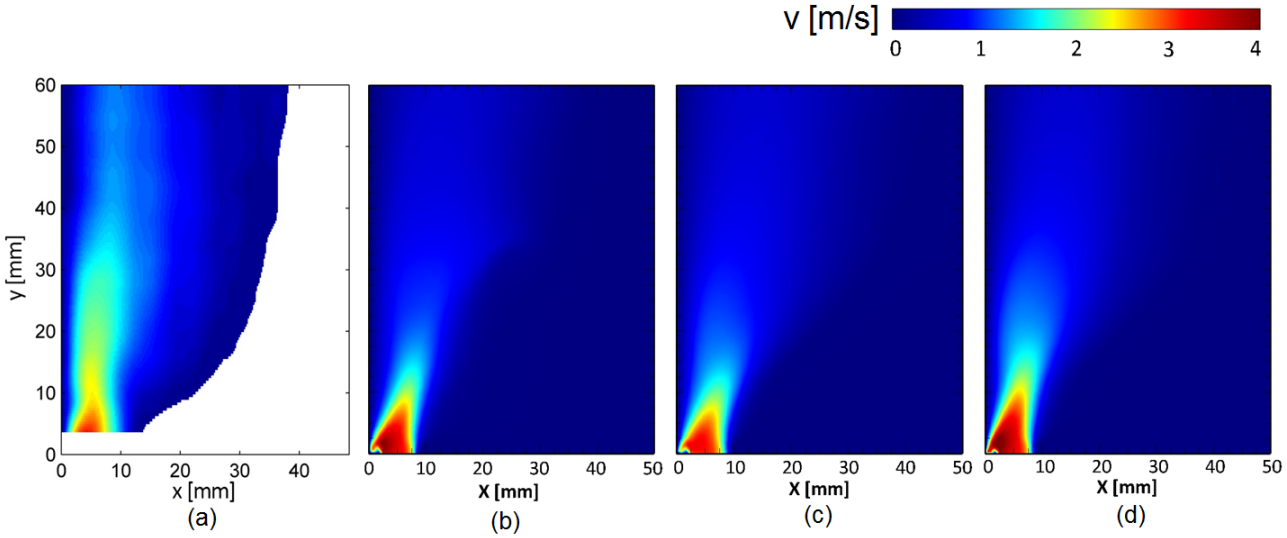

FIGURE 7. FLOW COMPARISONS - TANGENTIAL VELOCITY PROFILE SHOWN FOR THE TURBULENCE MODELS (a) EXPERIMENTS, (b) ED, (c) FGM AND (d) SLF

with the experimental results in Fig. 8(a).

The case with ED model in Fig. 8(b) presents as maximum temperature value of 1650°C. The temperature contour underlines a very narrow profile compared to the experiments. Due to the fact that the experimental flame is unconfined, the entrainment of air is simulated through the pressure outlet conditions set at the walls and at the cylindrical geometry outlet that ensure an ambient air back-flow in the simulations. Also a DO radiation model is adopted in the numerics. In the experimental case at the burner exit, the flame presents a local rich equivalence ratio that reaches the lean value Φ=0.66 at the cylindrical geometry outlet. Figure 11(a) shows the OH* light emission that is located at a distance d=25-30 mm from the burner exit where the main reaction zone occurs. The exhaust gases are then mixed and diluted with ambient air due to the unconfined flame, bringing therefore to reduced temperature. Also the recirculation of exhaust gases performed in the experiments contributes to cool down the flame. In the simulations the rich core of the flame at the burner exit reacts with the cooling air and ambient air that oxidize with the remaining hydrocarbons leading to higher temperature compared to the experiments and increased axial length of the reaction zone. This process could be caused by a reduced mixing with ambient air

compared to the experiments leading to higher equivalence ratio and therefore higher temperature than in the measurements. The increased length of the reaction zone is evident in Fig. 11(b) and Fig. 11(c) where the highest OH* mole fraction is concentrated along the whole burner axial length. This phenomenon is shown also through the contours of mass fraction Y of CH_4 and CO_2 presented for all models in Fig. 9 and Fig. 10. These results lead to the assumption of an after-burning process in the simulations that brings to higher temperature and increased axial length of the reaction zone. The ED model, due to the fast chemistry assumption, can also lead to increased temperature values. In the simulation with ED model, the maximum temperature value is observed at d=15 mm from the burner exit, contrary to the experiments where it occurs at height d=25 mm.

The swirl numbers values at the outlet of the burner and at d=9 mm are slightly lower compared to the experiments. A lower swirl number is determined also at the axial position d=18 mm. The value at the position d=18 mm is not an accurate result for calculating the total swirl number, since it assumes a constant radius and a constant density in the combustion process. The parameters S_x and S_z show asymmetrical values in the cold flow simulations, contrary to the results with combustion where the values at each axial position are identical. The reason could be related to the combustion process, the uniform temperature and the increased velocity as well as the high density gradients, that lead to symmetrical streamlines. Also numerical diffusion could play a role. An averaged swirl number of S =0.40 is achieved in the ED model simulation, which represents a deviation of 15% from the experiments. Evaluating the mass flow balance between inlet and outlet of the burner, 99.66% of the total CH_4 has been burned in this combustion process. The solution with this model is an acceptable approximation, even if the main disadvantages concern the fast combustion process and the fact that secondary species as OH* are not considered.

The FGM contours are presented in Fig. 6(c), Fig. 7(c) and Fig. 8(c). The absolute velocity field in Fig. 6(c) has a similar shape compared to the experiments. It shows a narrow profile generated by the swirl-induced jet opening in the lower region at the burner exit. The combustion process provokes a gas expansion that leads to an opening contour at about d= 20 mm at the same position of the measurements. The highest absolute velocity at about d=30 mm does not coincide with the position of the highest temperature values. The main reaction zone and the maximum temperature are located at higher axial position d=40 mm compared to the ED model (see Fig. 8(c). This could be attributed to the Pressure-Based Solver, since it first solves the momentum and the pressure correction equations, and then the energy equation that calculates the temperature value. The maximum temperature value of 1725° C is reached in this simulation. As explained before for the ED case, the rich flame core at the burner exit is mixed with the cooling air and the ambient air leading to a lean equivalence ratio. The cooling air and ambient air that oxidize with the remaining hydrocarbons provoke higher temperature compared to the experiments and increased axial length of the reaction zone (see plots of mass fraction of CO_2 in Fig. 10 shown for all numerical models). Due to this outcome an after-burning process in the simulations is assumed. A valuation of the intermediate species formed is possible using the FGM model. A validation of the released OH* in Fig. 11 during the combustion process is performed with the experimental data. The OH* radicals contours obtained for the simulations and the experiments are presented in Fig.11. Figure 11(a) shows the average light emission of the OH* radical in the investigated swirl-stabilized flame. The excited OH* in the heat release region are highlighted in the experiments. The chemiluminescence is used as a marker for the heat release. The OH* light emission in the experiments does not have units. For this reason only a qualitative comparison between the numerical results and the experiments can be carried out. In the numerical simulations the OH* mole fraction produced amount is represented. The OH* released associated to the temperature profile for the FGM case is shown in Fig. 11(b). OH* radicals measured in the experiments are due to ultraviolet (UV) chemiluminescence. This technique underlines the position of the maximum heat release, while the FGM profile illustrates the production of this radical during the reactions and reflects the spatial concentration. In the simulations the excited OH* in the heat release zone could not be isolated. For this reason in the numerics the mole fraction of OH* present in the postflame region is also evident. The position of the maximum OH* concentration and not the shape of the respective profile can be used to compare numerics with experiments.
In this model, a progress variable and its variance are introduced in addition to the mixture fraction. These variables can also influence the flame position. The determination of the variance is obtained by means of an additional transport equation, that can lead to a temperature deviation and consequently to a temperature increase. An alternative possibility would be to solve the progress variable variance with an algebraic approach [25].
The profile of the absolute velocity for the SLF model in Fig. 6(d) underlines a very accurate behavior compared to the measurements. The velocity contour in the range d=25-40 mm presents values up to U=3.5 m/s showing a similar trend to the measurements. Lower velocity values compared to the experiments are reached beyond d=40 mm. The temperature field presents higher values compared to the experimental investigation as highlighted in Fig.8(d). The highest temperature of 1650°C can be related to an after-burning process, resulting in an additional temperature increase. The temperature profile shape is the most accurate compared to the experiments but it shows the maximum temperature at higher axial direction. The hybrid formulation adopted in the paper that includes a transport equation for the reaction progress variable in the SLF approach, could represent the reason for the most accurate results performed by the current SLF model applied. The progress variable variance is

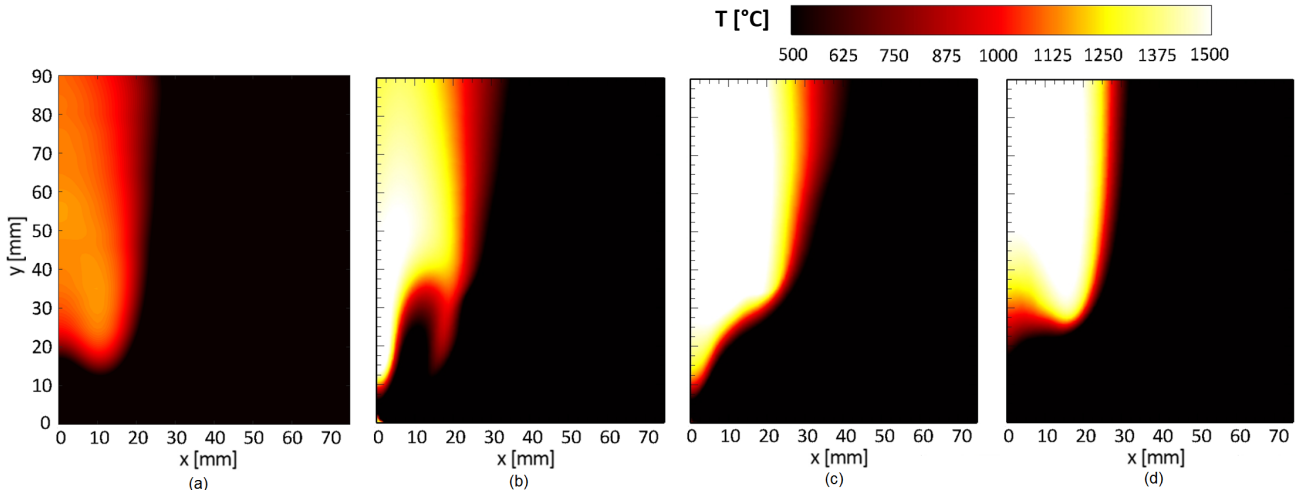

FIGURE 8. FLOW COMPARISONS - TEMPERATURE PROFILE SHOWN FOR THE COMBUSTION MODELS (a) EXPERIMENTS, (b) ED, (c) FGM AND (d) SLF

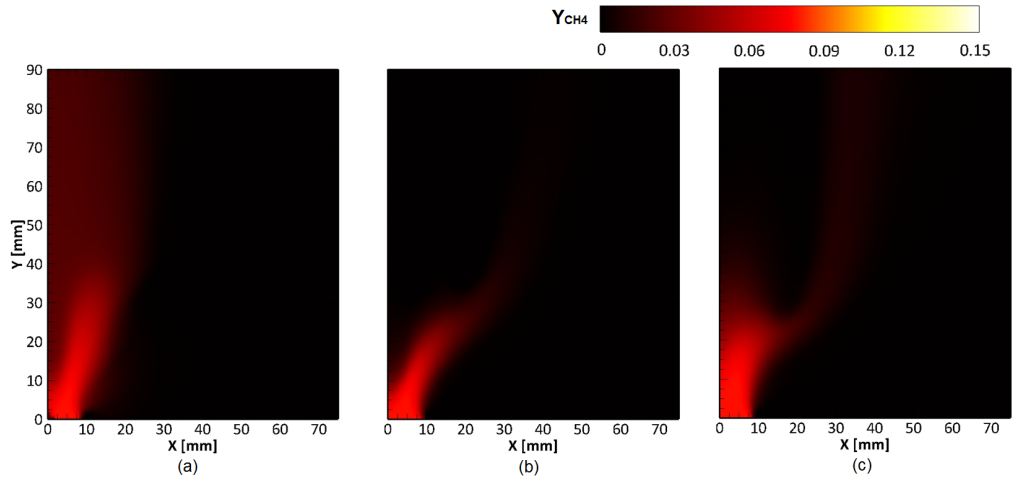

FIGURE 9. FLOW COMPARISONS - MASS FRACTION OF CH4 SHOWN FOR THE COMBUSTION MODELS (a) ED, (b) FGM AND (c) SLF

not considered in this model contrary to FGM. A deviation between the position of the maximum velocity values and the highest temperature is observed, that is probably due to the spatial discretization process and solving procedure. The OH* radicals in Fig. 11(c) are formed at height d=30 mm in the axial direction and x=10 mm in the radial direction. They are produced at higher position compared to the experiments matching the highest temperature position. The swirl numbers at the burner outlet and at d=9 mm present the same values as in the experimental results. The swirl number values in the x-direction and the z-direction are also symmetrical, due to the combustion influence.

Figure 12 and Fig. 13 show the absolute velocity and temperature trends for all simulations with the different combustion models and for the experiments along a line taken at x=7 mm. A polynomial line has been also considered to represents the experimental curve behavior. The diagram in Fig. 12 shows an accurate approximation of the FGM and SLF flamelet approaches with the experiments. For all numerical models the velocity values are increasing at the burner exit due to the swirl-induced jet opening reaching values of about U=5 m/s at d=8 mm but sligthly lower than the experiments. The velocity profile underlines a decreased behavior in the range between d=10-20 mm in the numerical and experimental cases. The velocity trend shows a good agreement between the experiments and the numerics with overall experimental values higher than in the simulations. FGM and SLF models present an increased velocity due to gas expansion

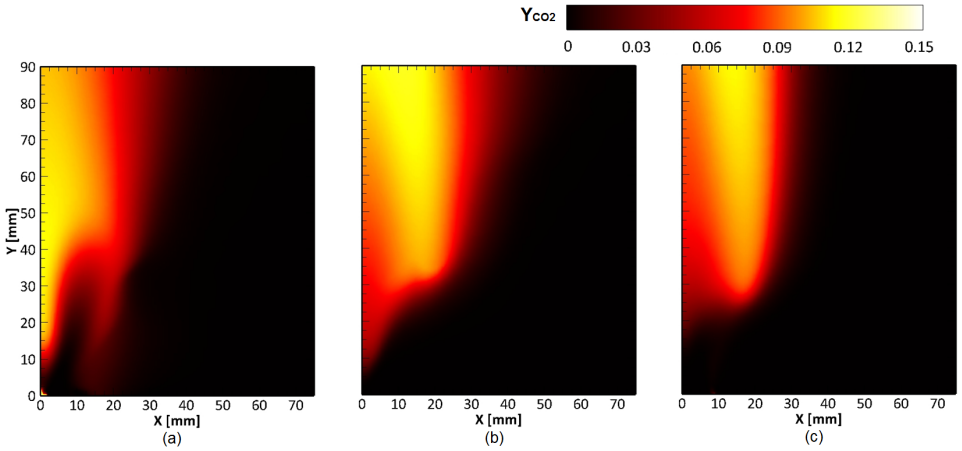

FIGURE 10. FLOW COMPARISONS - MASS FRACTION OF CO2 SHOWN FOR THE COMBUSTION MODELS (a) ED, (b) FGM AND (c) SLF

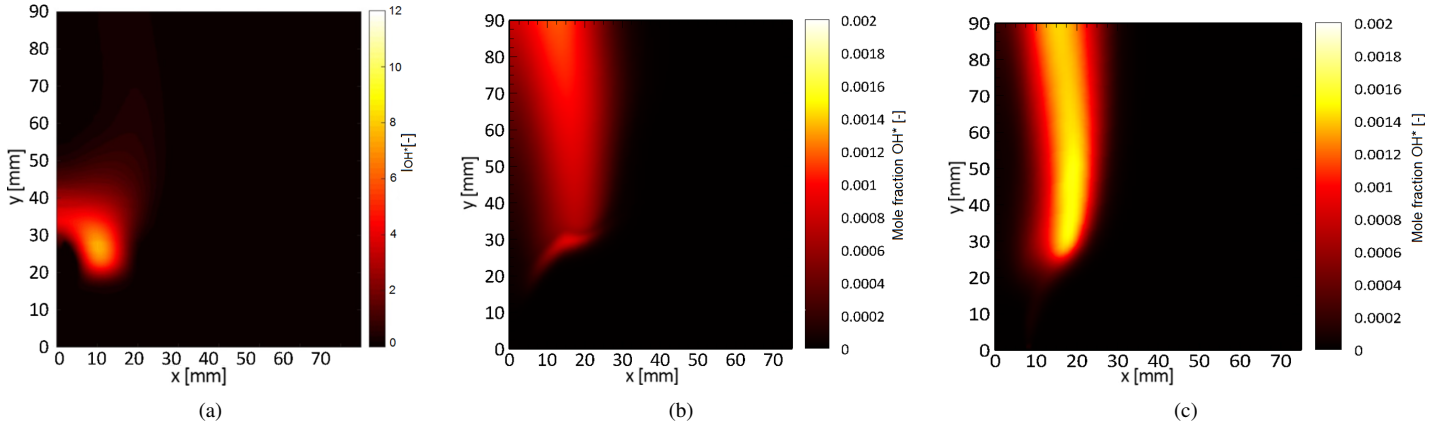

FIGURE 11. OH* RADICAL PROFILE SHOWN FOR THE COMBUSTION MODELS (a) EXPERIMENTS, (b) FGM AND (c) SLF

in the range d=20-40 mm matching in an accurate way the experimental profile but maintaining lower values of about U=3.5 m/s compared with the experiments. The ED model contrary to the other numerical models does not predict the increased velocity in the range d=20-40mm due to its assumption of fast chemistry model (see also contour plot in Fig. 6(b)). The highest temperature positions reached in the experiments and in the simulations can be clearly observed in the diagram in Fig. 13. In the experiments the highest temperature value of 1200°C is reached at a position d=25 mm. The simulations present higher temperature values compared to the experimental data in the range T=1550-1700°C. The highest temperatures in all simulations are observed further downstream in comparison with the experiments at positions beyond d=30 mm as also shown in Fig. 8. Figure 14 and Fig. 15 present the absolute velocity and temperature trends for all simulations with the different combustion models and for the experiments along the centerline in order to give a more accurate representation of the flame position. The velocity behavior shows a quite good agreement between the experiments and the two flamelets models. FGM almost matches the measurements at about d=25 mm reaching velocity values of U=1.8 m/s. SLF shows similar velocity values compared to the experiments but at a position slightly shifted to d=32 mm. ED presents too high velocities already in the range d=10-20 mm underlying the fact that the reactants start immediately to burn when coming into contact with each other. Figure 15 shows a good agreement between the experiments and the SFL model. SLF presents the same trend as the measurements until about d=25 mm, but it reaches higher temperature compared to the experiments in the range above d=30 mm. FGM underlines the same trend as SLF but with higher temperature values. The averall more accurate representation of the experiments compared to the other models

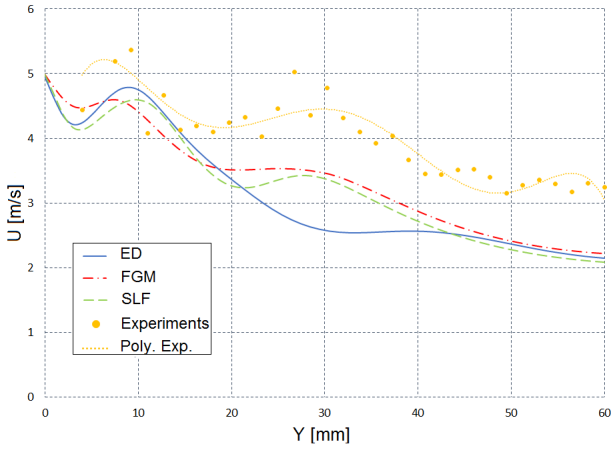

FIGURE 12. ABSOLUTE VELOCITY BEHAVIOR SHOWN AT x=7 mm FOR THE COMBUSTION MODELS AND FOR THE EXPERIMENTS

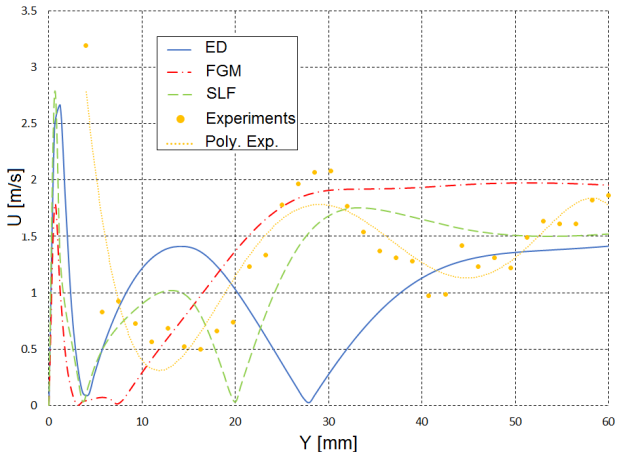

FIGURE 14. ABSOLUTE VELOCITY BEHAVIOR SHOWN AT THE CENTERLINE FOR THE COMBUSTION MODELS AND FOR THE EXPERIMENTS

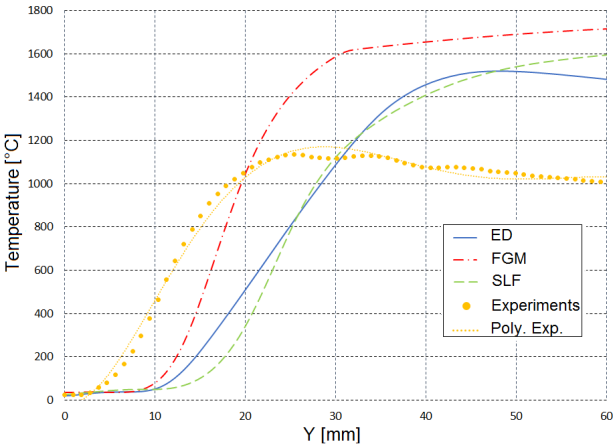

FIGURE 13. TEMPERATURE BEHAVIOR SHOWN AT x=7 mm FOR THE COMBUSTION MODELS AND FOR THE EXPERIMENTS

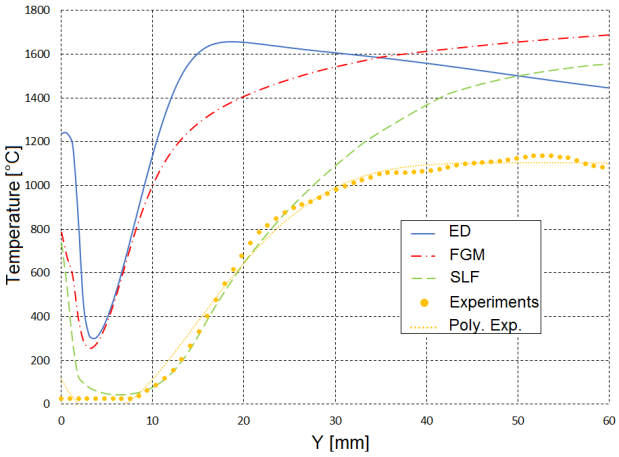

FIGURE 15. TEMPERATURE BEHAVIOR SHOWN AT THE CENTERLINE FOR THE COMBUSTION MODELS AND FOR THE EXPERIMENTS

performed by the SLF is related to the new formualtion that includes the reaction progress variable C equation into the flamelet SLF approach.

CONCLUSION

In this work a geometry burner is investigated numerically with the CFD code *FLUENT*.
Three different turbulence models are used for the cold flow simulations and results are compared to PIV measurements. The model reliazable k-ε represents more accurate velocity behavior compared with experiments and it shows the best agreement with PIV data. Also the swirl numbers values calculated for all cold flow simulations at the burner exit and at d=9 mm show an accurate trend compared to the experimental tests. Calculations are performed in order to compare the combustion modeling influence on the velocity and temperature profiles. In the case with ED model the combustion process takes already place at axial position d=15 mm, due to the model assumption of fast chemistry. A maximum temperature value of 1650° C is reached, which represents a difference of about 500° C compared to the measurements. This increased temperature can be attributed to the after-burning process as well as to the model properties. The absolute velocity profile for the FGM model shows an accurate shape and behavior compared to the experiments, but an higher maximum temperature value is determined.

Both models with flamelet approach as FGM and SLF, present the most accurate agreement in terms of velocity profiles, position of highest velocity and temperature values, OH* production and the swirl number trend compared to the measurements. The new formualtion that includes the progress variable C equation into the flamelet SLF approach leads to more accurate results performed by SLF. A deviation of the absolute velocity profile from the temperature profile is observed in the simulations. This can be attributed to the pressure-based solver.
In this work the ability of current state-of-the-art RANS modeling is documented. Potential for further improvement lies in the application of more reliable numerical methods. The results of this study are considered as preliminary results with the aim to perform following (Large Eddy Simulation) LES simulations to better predict the combustion and premixed processes. The next step concerns an accurate sensitivity analysis of the chemical reactions and of the products that contribute strongly to the temperature increase or are formed in high concentration. The mechanism used should be adapted modifying the Arrhenius constants to determine the reaction rate (see work of Prieler et al. [32]). As outlook of the current study, also the available measurements of heat release fluctuations induced by a siren should be compared with transient unsteady simulations in order to perform an acoustic analysis of the oscillations influencing the flame and the flow field.

ACKNOWLEDGEMENTS

The project is a Lead-Agency D-A-CH project in cooperation between Graz University of Technology, Austria and Technische Universität Dresden, Germany, and was funded by the Austrian Science Fund FWF within Grant No. FWF-I2544-N30.

REFERENCES

[1] Lucca-Negro, O., and O′Doherty, T. "Vortex breakdown: a review". *Prog. Energy Combustion Sci.,* ***27***(4), p. 431.

[2] Huang, Y., and Yang, V., 2009. "Dynamics and stability of lean-premixed swirl-stabilized combustion". *Prog. Energy Combustion Sci.,* ***35***(4), pp. 293–364.

[3] Sattelmayer, T., and Polifke, W., 2003. "Assessment of methods for the computation of the linear stability of combustors". *Combustion Science and Technology,* ***175***(3), pp. 453–476.

[4] Schuermans, B., Guethel, F., Pennell, D., Guyot, D., and CO, P., 2010. "Thermoacoustic modeling of a gas turbine using transfer functions measured under full engine pressure". *Journal of Engineering for Gas Turbines and Power,* ***106***(11).

[5] Peterleithner, J., Marn, A., and Woisetschläger, J., 2015. "Interferometric investigation of the thermoacoustics in a swirl stabilized methane flame". In In Proceedings of GT2015, ASME Turbo Expo 2015, Montreal, Canada.

[6] Lauer, M., 2011. "Determination of the Heat Release Distribution in Turbulent Flames by Chemi-luminescence Imaging". PhD Thesis, University of Technology Munich.

[7] Peterleithner, J., Stadlmair, N., Woisetschläger, J., and Sattelmayer, T., 2016. "Analysis of measured flame transfer functions with locally resolved density fluctuation and oh-chemiluminescence data". *Journal of Engineering for Gas Turbines and Power,* ***138***(3).

[8] Peterleithner, J., Basso, R., Heitmeir, F., Woisetschläger, J., Schlüssler, R., Czarske, J., and Fischer, A., 2016. "Comparison of flame transfer functions acquired by chemiluminescence and density fluctuation". In In Proceedings of GT2016, ASME Turbo Expo 2016, Seoul, South Korea.

[9] Abou-Taouk, A., Whiddon, R., Sigfrid, I., and Eriksson, L., 2011. "Cfd investigation of swirl-stabilized flexi-fuel burner using methane-air mixture for gas turbines". *ISABE*, pp. 2011–1122.

[10] Hatziapostolou, A., Orfanoudakis, N., Koukou, M., and Raptis, G., 2006. "Cfd modeling of the swirl-stabilised flame produced by a laboratory-scale combustor: selection of the turbulence model". In Proceeding of the 4th WSEAS Int. Conf. on Heat Transfer, Thermal Engineering and Environment, pp. 83–88.

[11] Van Oijen, J., Donini, A., Bastiaans, R., ten Thije Boonkkamp, J., and de Goey, L., 2016. "State-of-the-art in premixed combustion modeling using flamelet generated manifolds". *Progress in Energy and Combustion Science,* ***57***, pp. 30–74.

[12] Shih, T., Liou, W., Shabbir, A., Yang, Z., and Zhu, J., 1995. "A new k-ε eddy viscosity model for high reynolds number turbulent flows". *Comput. Fluids,* ***24***, pp. 227–238.

[13] Magnussen, B., and Hjertager, B., 1976. "On mathematical modelling of turbulent combustion with special enphasis on soot formation and combustion". In Proceedings of the Combustion Institute, Vol. 16, pp. 719–729.

[14] Peters, N. "Laminar diffusion flamelet models in non-premixed turbulent combustion". *Prog. Energy Combustion Sci.,* ***10***(3), p. 319.

[15] Law, W., and Gimbun, J., 2015. "Influence of nozzle design on the performance of a prtial combustion lance: A cfd study". *Chemical Engineering Research and Design*, pp. 104–558.

[16] Magnussen, B., 1981. "On the structure of turbulence and a generalized eddy dissipation concept for chemical reaction in turbulent flow". *19th AIAA Meeting. St. Louis, USA*.

[17] Lysenko, D., Ertesvag, I., and Rian, K., 2014. "Numerical simulation of non-premixed turbulent combustion using the eddy dissipation concept and comparing with the steady laminar flamelet model". *Flow, Turbulence and Combustion,* ***93***(4), p. 577.

[18] Puggelli, S., Bertini, D., Mazzei, L., and Andreini, A. "Scale adaptive simulations of a swirl stabilized spray flame using flamelet generated manifold". *Energy Procedia,* ***101***, p. 1143.

[19] Giuliani, F., Woisetschläger, J., and Leitgeb, T., 2012. "Design and validation of a burner with variable geometry for extended combustion range". In In Proceedings of GT2012, ASME Turbo Expo 2012, Copenhagen, Denmark.

[20] March, M., 2017. "Auslegung, Konstruktion und Validierung eines Versuchsbrenners mit drallstabilisierter Flamme und optisch transparenter Brennkammer". Master's thesis, University of Technology Graz.

[21] Peterleithner, J., Salcher, F., and Woisetschläger, J., 2014. "Frequency resolved interferometric detection of local density fluctuations in flames". In Proc. 17th International Symposium on Application of Laser Techniques to Fluid Mechanics, Lisbon.

[22] Pretzler, G., Jäger, H., Neger, T., Philipp, H., and Woisetschläger, J., 1992. "Comparison of different methods of abel inversion using computer simulated and experimental side-on data". *Z. Naturforsch.,* ***47a***, pp. 955–970.

[23] Raffel, M., 2015. "Background-oriented schlieren (bos) techniques". *Experiments in Fluids,* ***56***, p. 60.

[24] Tanneberger, T., Reichel, T., Krüger, O., Terhaar, S., and Paschereit, C., 2015. "Numerical investigation of the flow field and mixing in a swirl-stabilized burner with a non-swirling axial jet". In In Proceedings of GT2015, ASME Turbo Expo 2015.

[25] Ansys, 2012. *ANSYS FLUENT theory guide*, ansys fluent release 14.5 ed.

[26] WestBrook, C., and Dryer, F., 1984. "Chemical kinetic modeling of hydrocarbon combustion". *Prog. Energy Combustion Sci.,* ***10***, pp. 1–54.

[27] Jones, W., and Lindstedt, R., 1988. "Global reaction schemes for hydrocarbon combustion". *Combustion and Flame,* ***73***, pp. 233–249.

[28] Novosselov, I., and Malte, P., 2008. "Development and application of an eight-step global mechanism for cfd and crn simulation of lean-premixed combustors". *Journal of Engineering for Gas Turbines and Power,* ***130***.

[29] WestBrook, C., and Dryer, F., 1981. "Simplified reaction mechanisms for the oxidation of hydrocarbon fuels in flames". *Combust Sci Technol.,* ***27***, pp. 31–43.

[30] Smith, G., Golden, D., Frenklach, M., Moriarty, N., Eiteneer, B., Goldenberg, M., Bowman, T., Hanson, R., Song, S., Gardiner, W., Lissianski, V., and Qin, Z. Tech. rep. See also URL `http://www.me.berkeley.edu/grimech/`.

[31] Lieuwen, T., 2012. *Unsteady Combustor Physics*. Cambridge Univ. Press. UK.

[32] Prieler, R., Mayr, B., Viehbock, D., Demuth, M., and Hochenauer, C., 2017. "Sensitivity analysis of skeletal reaction mechanisms for use in cfd simulation of oxygen enhanced combustion systems". *Journal of the Energy Institute,* ***91***, pp. 369–388.